Effect of the oxygen content in solution on the static and cyclic deformation of titanium foams

Lefebvre, L.-P.; Baril, É.; Bureau, M. N.

Publisher's version / la version de l'éditeur:
Journal of Materials Science: Materials in Medicine, 20, 11, pp. 2223-2233, 2009

Web page / page Web
http://dx.doi.org/10.1007/s10856-009-3798-x
http://nparc.cisti-icist.nrc-cnrc.gc.ca/npsi/ctrl?action=rtdoc&an=10820125&lang=en
http://nparc.cisti-icist.nrc-cnrc.gc.ca/npsi/ctrl?action=rtdoc&an=10820125&lang=fr

J Mater Sci: Mater Med
DOI 10.1007/s10856-009-3798-x

Effect of the oxygen content in solution on the static and cyclic deformation of titanium foams

L. P. Lefebvre · E. Baril · M. N. Bureau

Received: 9 January 2009 / Accepted: 2 June 2009

Abstract It is well known that interstitials affect the mechanical properties of titanium and titanium alloys. Their effects on the fatigue properties of titanium foams have not, however, been documented in the literature. This paper presents the effect of the oxygen content on the static and dynamic compression properties of titanium foams. Increasing the oxygen content from 0.24 to 0.51 wt% O in solution significantly increases the yield strength and reduces the ductility of the foams. However, the fatigue limit is not significantly affected by the oxygen content and falls within the 92 MPa ± 12 MPa range for all specimens investigated in this study. During cyclic loading, deformation is initially coming from cumulative creep followed by the formation of microcracks. The coalescence of these microcracks is responsible for the rupture of the specimens. Fracture surfaces of the specimens having lower oxygen content show a more ductile aspect than the specimens having higher oxygen content.

1 Introduction

Porous titanium coatings have been used for many years in different load bearing orthopedic applications. These surfaces were initially proposed in the late 60's as a solution to problems encountered with methacrylate-based bone cement used for orthopedic implant fixation [1, 2]. These coatings have high roughness, increase the friction between the implant and surrounding bone and provide the initial stability to the implants. Besides, the interconnected porosity allows bone tissue ingrowth that secures the long-term fixation and stability of the implant. This approach is now widely used in various hip and knee cementless procedures and most orthopedic implant manufacturers are now commercializing implants with these coatings.

Research has recently switched from thin porous bead coatings, sintered mesh and thermal sprayed rough coatings to metallic foams. These foams have been used in the development of various new and improved treatments such as bone augmentation and graft free vertebra fusion for the treatment of degenerative disk diseases. These foams have the advantage of being much more porous than the traditional sintered beads or mesh and plasma spray coating. The increased porosity provides elastic modulus much closer to those of bones, more space for bone in-growth and interlocking as well as more surface for bone-implant contact.

It is well established that the mechanical properties of dense titanium and titanium alloys are sensitive to the presence of interstitial solutes such as oxygen, nitrogen, carbon and hydrogen. These interstitials increase the elastic modulus, the yield strength and reduces the ductility of titanium and titanium alloys [3]. Nitrogen has generally the most significant effect, followed by oxygen and carbon. While nitrogen and carbon are usually not found at high concentration in dense titanium, oxygen is a common contaminant due to the high affinity of titanium for oxygen and its high solubility in titanium. At low concentration, oxygen occupies octahedral sites of the α-titanium crystal and increases the lattice parameters as well as the c/a ratio in the crystal, resulting in a volumetric change of 0.0013 nm^3 per atomic percent of oxygen [4, 5]. The oxygen atoms interact with the hydrostatic stress field of the dislocations but also with the shear stress field, so that

L. P. Lefebvre (✉) · E. Baril · M. N. Bureau
National Research Council Canada/Industrial Materials Institute,
75 de Mortagne, Boucherville, QC J4B 6Y4, Canada
e-mail: louis-philippe.lefebvre@cnrc-nrc.gc.ca

Journal : Large 10856 Dispatch : 10-6-2009 Pages : 11
Article No. : 3798 LE TYPESET

both edge and screw dislocation motions are affected. Therefore, increasing oxygen content results in an increase of the yield strength, hardness and fatigue resistance at a given stress level, whereas it decreases the ductility and impact resistance by restricting twinning and prismatic slip [6].

Since interstitials significantly affect the properties of titanium, standards have been established on the chemical requirements for the use of dense titanium in orthopedic and dental applications [7–11]. A standard has also been developed for porous titanium coating for the production of surgical implants [12]. According to this standard, the maximum content of oxygen in the powder used for such coatings must be lower than 0.4 wt% O. The standard does not, however, specify the amount of oxygen in solution in the final coating.

The effect of porous coating on the fatigue properties of Ti–6Al–4V implants have been reported in the literature [13–15]. It is recognized that porous coating reduces the fatigue strength of the implants. This reduction is associated with the modification of the microstructure during the high temperature sintering treatment as well as with the stress concentration coming from the surface irregularities at the sintered bond sites on the surface of the implants. The fatigue properties of tantalum and nickel-titanium foams intended for biomedical applications have also been reported in the literature. The compressive fatigue limits reported by [16–18] are 7.5 MPa at 10^8 cycles for 63–68% open porosity nickel-titanium foams and 13.2 MPa at 10^8 cycles for 65–70% open porosity tantalum foams. In another study by [19], the compressive fatigue limit of 75–85% porous tantalum foams is around 23 MPa at 5×10^6. Variations in the results presented in the later study were significant and reported to be dependant upon the nature of the material tested.

No studies are available on the fatigue properties of pure titanium foams as well as on the effect of the oxygen content on the fatigue of these materials. This probably comes from the fact that these materials are relatively new. The limited information available can also be attributed to challenges associated with the production of materials with the exact same structure but with different level of oxygen in solution. Difficulties also come from the discrimination of the amount of oxygen in solution from the oxygen in the oxide layer on the surface of the foam. Due to the high specific surface area of the materials, the relative contribution of the amount of oxygen coming from the oxide formed on the surface of the foam must be taken into account when determining the effect of oxygen on the properties of these materials.

This paper describes the compression static and dynamic properties of titanium foams having different oxygen contents. The titanium foam was produced with a powder metallurgy process. The foam samples were oxidized at low temperature to obtain different oxygen concentrations. They were then treated at 1000°C to dissolve the surface oxide and obtain solid solutions with different oxygen levels. The resulting titanium foam samples showed the same structure but different oxygen contents. They were then tested in compression under static (monotonic and creep at room temperature) and cyclic loading to investigate the effect of oxygen on their properties. The fatigue behavior of the titanium foams was done under compression-compression fatigue, i.e. with a non-zero mean stress.

2 Experimental procedure

Titanium foams were produced using a process described elsewhere [20]. Briefly, spherical pure titanium powder (AP&C Advanced Powders and Coatings Inc., Quebec, Canada; −180 μm) was admixed with a polyethylene binder and a chemical foaming agent (p,p'-oxybis[benzenesulfonyl hydrazide]). The resulting powder mixture was poured into a cylindrical mold and heated up in air at 210°C to foam the material. The resulting material was then successively debinded at 450°C in Ar (10^{-8} ppm O_2) and sintered at 1400°C under vacuum (10^{-5}–10^{-6} Torr range). To increase their oxygen content, the resulting foam cylinders were treated in Ar-20% O_2 at 3 different temperatures (300–450°C). Using this method, foams with 3 different oxygen concentrations were produced. Material A refers to the foam with the lowest oxygen content in solution (0.24 wt%), Material B is the foam with the intermediate oxygen content (0.42 wt% in solution) while material C refers to the foam with the highest oxygen concentration (0.51 wt% O in solution). The oxidized cylinders were solution treated for 1 h at 1000°C to dissolve the oxide layer and bring the oxygen into solid solution in titanium. After cooling, a thin oxide layer was reformed on the Ti surface (typically 5 nm, as described in [21]). Table 1 summarized the properties of the foams characterized in this study.

The density of the specimens was evaluated using the weight (Ohaus, Explorer, 210 g ± 0.1 mg) and physical

Table 1 Characteristics of the titanium foams characterized in this study

	A	B	C
Density (% theoretical)	51	51	51
Surface area (m^2/g)	0.05	0.05	0.05
Total oxygen content (wt%)	0.3	0.48	0.57
Oxide thickness (nm)	5	5	5
Oxygen in solution (wt%)	0.24	0.42	0.51
Yield strength (MPa)	129	162	178

Journal : Large 10856 Dispatch : 10-6-2009 Pages : 11
Article No. : 3798 LE TYPESET

dimensions of the cylinders. Specimens were observed with an optical microscope, a JEOL 6100 scanning electron microscope (SEM), an Hitachi S-4700 field-emission gun scanning electron microscope (FEG-SEM) and a X-Tek HMXST 225 X-ray microtomograph (μCT). The specific surface area was evaluated by gas adsorption (BET) using a Micrometrics ASAP 2010 system with krypton as adsorbate. Oxygen content was evaluated using an inert gas fusion technique with a LECO TCH-600 analyzer. The amount of oxygen in the oxide film was estimated using a method described in [21] based on the evaluation of the weight gain associated with the formation of the oxide film after the sintering treatment. The amount of oxygen in solution was deducted from the total measured amount of oxygen (LECO) and the estimated amount of oxygen in the oxide film. Compression testing was done on a MTS 100 kN testing machine. Cyclic tests were done under sinusoidal 10 Hz cycling (deformation rate of approximately 1 mm/s) and a load ratio ($R = \sigma_{min}/\sigma_{max}$) of 0.1. The tests were ended either at a user defined deformation of 22.5% or at 5×10^6 cycles (defined as no rupture). The cyclic tests were done on 11 specimens for materials A and B and 6 specimens for material C. Monotonic tests were performed at a crosshead speed of 1.25 mm/min to determine the effect of oxygen on the yield strength. Some tests were interrupted at 22.5% deformation to compare the level of damage (i.e. cracks) in the specimens deformed monotonically with those deformed under cyclic loading. Creep tests were also done under a static load (107 MPa) to determine the creep contribution to the total deformation under cyclic loading. All tests were done at room temperature in air. Cumulative deformation and deformation amplitude were measured using a platen-mounted LVDT transducer (Intertechnology, Don Mills, Canada, model 0243-000).

3 Results

A general view of the cylinders before compression is presented in Fig. 1. The specimens are 51% dense and consisted in a continuous network of open porosity. The pore diameters are typically between 50 and 400 μm, as determined visually on the SEM micrographs. Pycnometry measurements showed that the porosity is completely open. Besides, the material has a granular structure associated with the powder metallurgy process used. Polished cross sections (Fig. 2) and SEM micrographs (Fig. 3a) reveal that the particles are well sintered together. At high magnification, fine surface features can be observed (Fig. 3b, d). These features were produced by thermal etching during sintering as a result of the evaporation/condensation and surface diffusion of titanium occurring at high temperature during sintering. These fine sub-micron features on the surface of the material account for its high specific surface area (0.05 m^2/g as evaluated by BET). Accordingly, due to the presence of the thin oxide film naturally formed on the surface of titanium (typically 5 nm in the present case), the thermal etching lines contribute to the total oxygen content of the material.

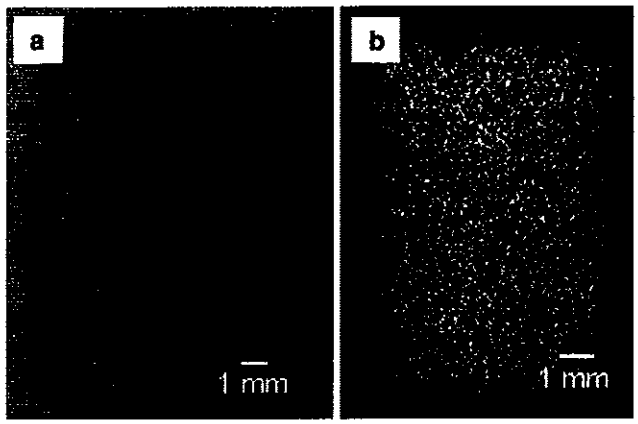

Fig. 1 Specimens characterized in the study **a** general view and **b** 2D cross section obtained from the reconstruction of microtomographic images

The total amount of oxygen in the specimens produced is 0.3, 0.48 and 0.57 wt% (Table 1). When the oxygen contribution of the natural oxide formed on the surface of titanium is taken into account (i.e. 0.06 wt%), the calculated amount of oxygen in solution are 0.24, 0.42 and 0.51 wt%. The total carbon content is approximately 0.3 wt%. Carbon comes mainly from the foaming agent decomposition products. Carbon present in the foaming agent reacts with titanium and forms biocompatible carbides during debinding and sintering (Fig. 2b). Table 1 summarizes the densities, surface area and composition of the foam samples characterized in this study.

The monotonic compression behavior of the foam cylinders containing 0.24 and 0.51 wt% O in solution is presented in Fig. 4. The curves are characteristic of compression curve of ductile porous materials showing three stages: the initial elasto-plastic loading, the plastic deformation plateau and the consolidation stage at the end of the compression tests. The vertical lines visible on the curve come from unloading done during the compression tests to evaluate the elastic modulus (not presented in this study). The shape of the curves changes when the oxygen content in solution increases. Indeed, the yield strength (defined in this study as the intersection of the lines parallel to the stage 1 and 2 in the monotonic compression curves) increases significantly when the oxygen content in solution increases, as reported in Fig. 5. In addition, the densification stage occurs at larger deformation and the slope of the

Journal : Large 10856 Dispatch : 10-6-2009 Pages : 11
Article No. : 3798 LE TYPESET

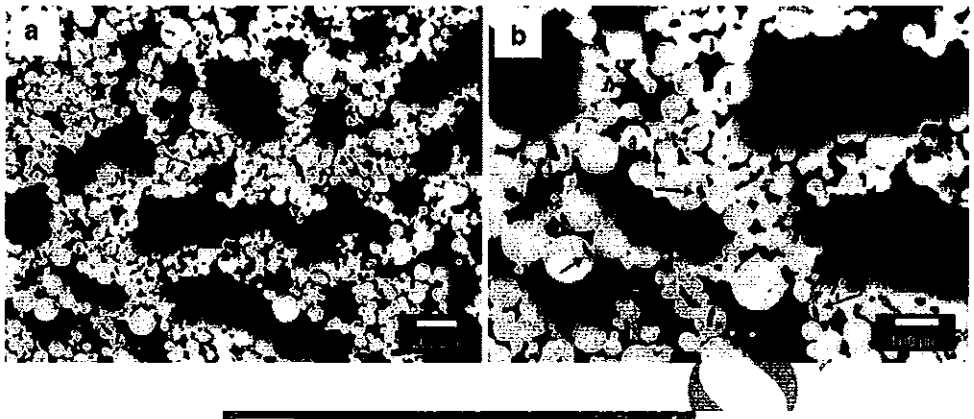

Fig. 2 Optical micrographs of the polished cross section of a 0.24 wt% O specimen: **a** low magnification and **b** high magnification micrograph with arrows pointing at carbides

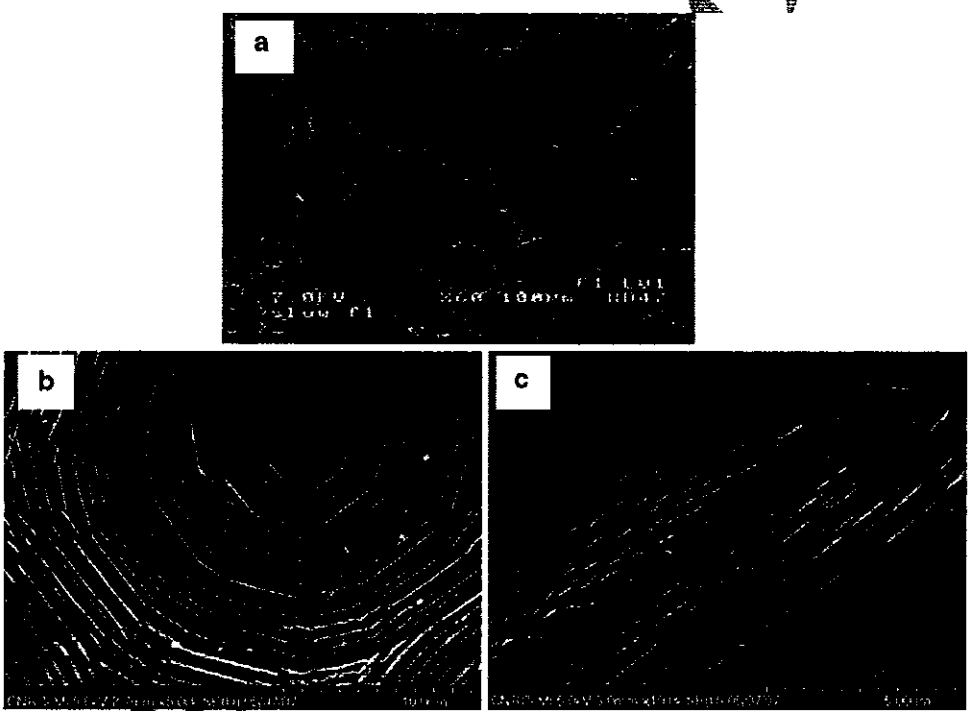

Fig. 3 SEM micrographs of a foam **a** low magnification, **b** high magnification presenting the etching lines on the surface of the particles and **c** high magnification showing a close-up at the submicronic thermal etching lines

densification is smaller when the amount of oxygen increases (Fig. 4).

While all specimens exhibited smooth curves typical of ductile foams, only the specimens containing small amount of oxygen (i.e. 0.24 wt%) deformed plastically up to the end of the tests. Indeed, when the amount of oxygen in solution is large, the specimens showed severe cracks and small pieces of material were ejected during the tests. Figure 6 presents specimens containing two oxygen contents (0.24% and 0.51 wt%) that were submitted to 22.5% deformation under monotonic loading, which is equivalent to the maximum deformation limit imposed during the fatigue tests done in this study. On one hand, the specimens with 0.24 wt% O did not show apparent cracks at their surfaces (Fig. 6a). The observation of the internal structure of these specimens using microtomography (Fig. 7a) and optical microscopy on polished cross sections (Fig. 7b) confirmed that only few microcracks were formed after

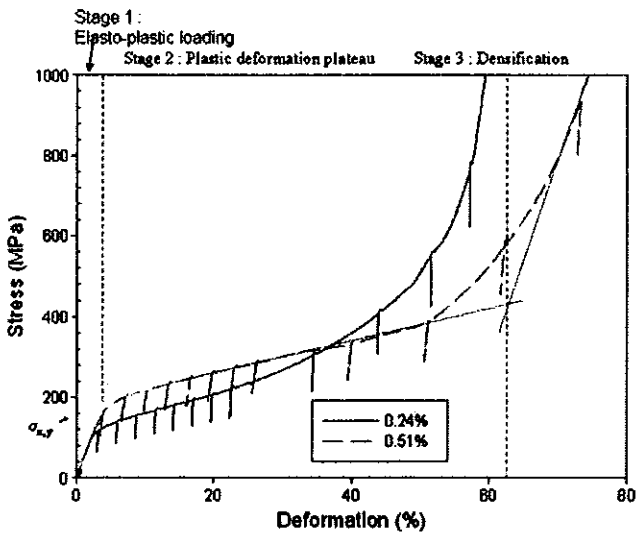

Fig. 4 Compression curves of titanium foams having two different oxygen contents in solution

Journal : Large 10856 Dispatch : 10-6-2009 Pages : 11
Article No. : 3798 LE TYPESET

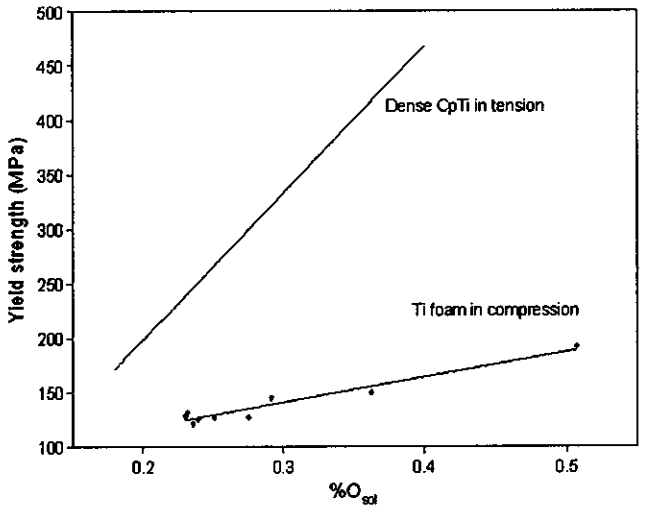

Fig. 5 Effect of oxygen content in solution on the yield strength of the Ti foams in compression and dense Ti in tension (from Refs. [7] and [21])

22.5% deformation in the 0.24 wt% O specimens. On the other hand, the specimens containing 0.51 wt% O in solution had significantly more cracks visible on their external surfaces (Fig. 6b) and in the internal structure after monotonic compression.

The cumulative cyclic deformation curves for specimens having two levels of oxygen in solution (0.24 and 0.51 wt% O) is presented in Fig. 8. At low stress level, the average deformation increases monotonically. The final cumulative deformation of the specimens is relatively low and similar for both oxygen contents. No crack or microcrack was observed on the external surfaces or polished cross sections. At higher stress levels, the cumulative deformation slowly raises up to a point where it strongly increases during the collapse stage.

The deformation amplitude at the beginning of the tests (Fig. 9) is similar and is not affected by the oxygen content because the elastic modulus is similar for all materials and the applied stress is lower than the materials yield strength. Prior to their collapse, the deformation amplitude is approximately constant, in agreement with the cumulative deformation curves shown in Fig. 8. However, during the collapse stage, an increase of the deformation amplitude is observed, again in agreement with the cumulative deformation curves shown in Fig. 8. It should be noted that the sudden decrease in deformation amplitude observed in some of the longer fatigue tests (i.e. $>1 \times 10^6$ cycles), as observed in the 0.24 wt% O specimen tested at 83 MPa, is related to a sudden displacement of the LVDT transducer during the fatigue tests due to a lack of lubricant used to prevent the friction between the pin and the cylinder of the LVDT transducer.

The specimens that failed during the fatigue tests (defined at 22.5% of cumulative deformation) show cracks on their external surface for all oxygen levels (Fig. 10a, b). Slices from μCT reconstruction showing the internal structure of specimens having 2 different oxygen contents (Fig. 10c, d) present the formation of crush bands and internal cracks (45° to the loading direction). Evidence of cell collapse in the direction parallel to the applied stress can also be observed. The metallographic cross sections show several microcracks distributed throughout the specimens (see arrows in Fig. 11). The crack propagation does not seem, however, to be affected by the presence of the carbides. In fact, the cracks propagate at the necks between former powder particles but also within the particles. Very few cracks are located in the vicinity of the carbides.

The total cumulative deformation as a function of the loading time for foam specimens containing 0.24 wt% O in solution tested at 107 MPa under cyclic loading (fatigue,

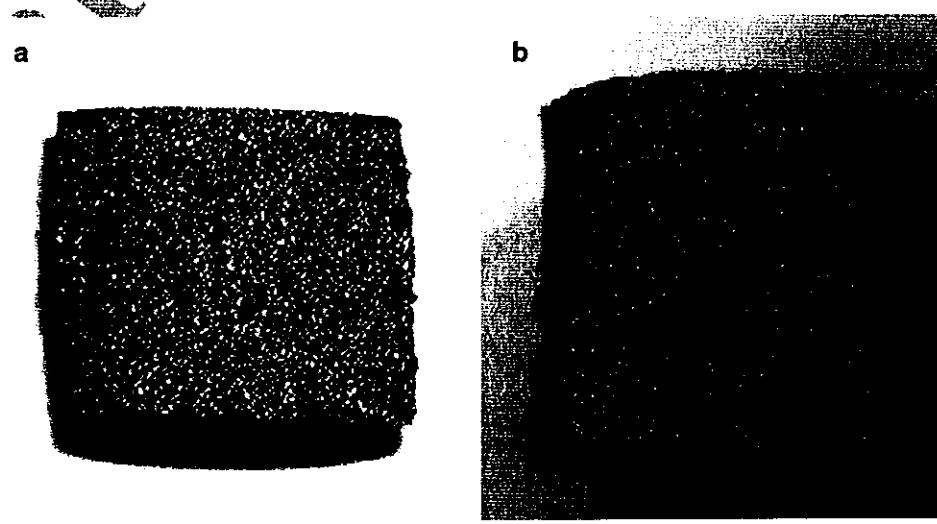

Fig. 6 General view of specimens after 22.5% deformation under monotonic compression: **a** 0.24 wt% O and **b** 0.51 wt% O specimens

Journal : Large 10856 Dispatch : 10-6-2009 Pages : 11
Article No. : 3798 LE TYPESET

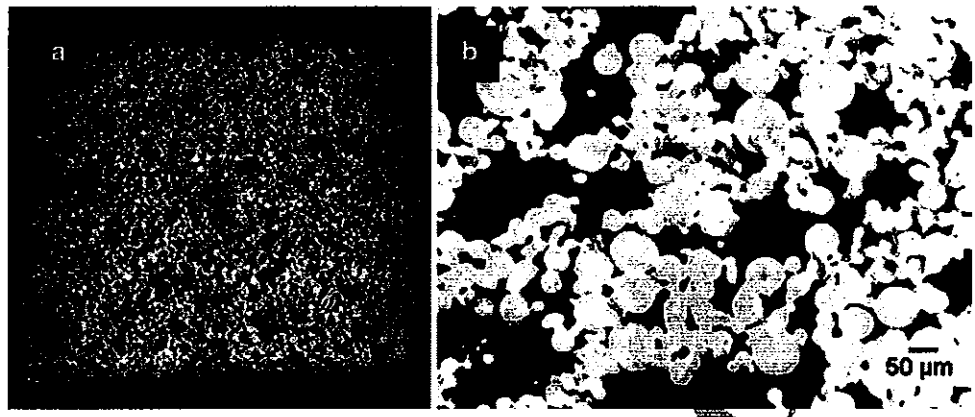

Fig. 7 Cross section of the 0.24 wt% O specimens after 22.5% deformation under monotonic compression **a** 2D microtomography cross section presenting the general view of the specimen and **b** polished cross section presenting a closer view of the microstructure

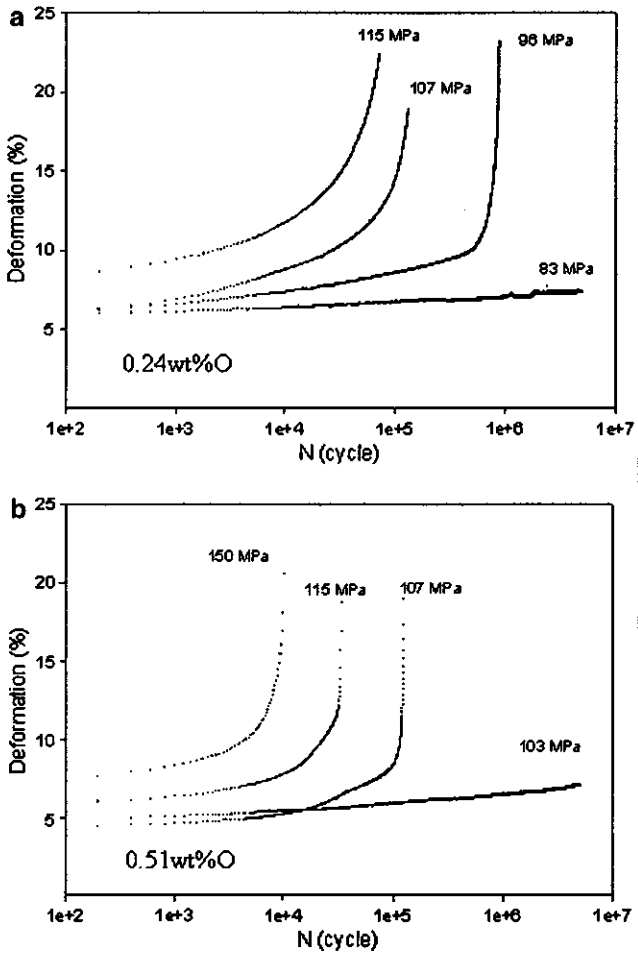

Fig. 8 Cumulative deformation versus cycle at different applied stresses for foams containing different amounts of oxygen in solution: **a** 0.24 and **b** 0.51 wt% O

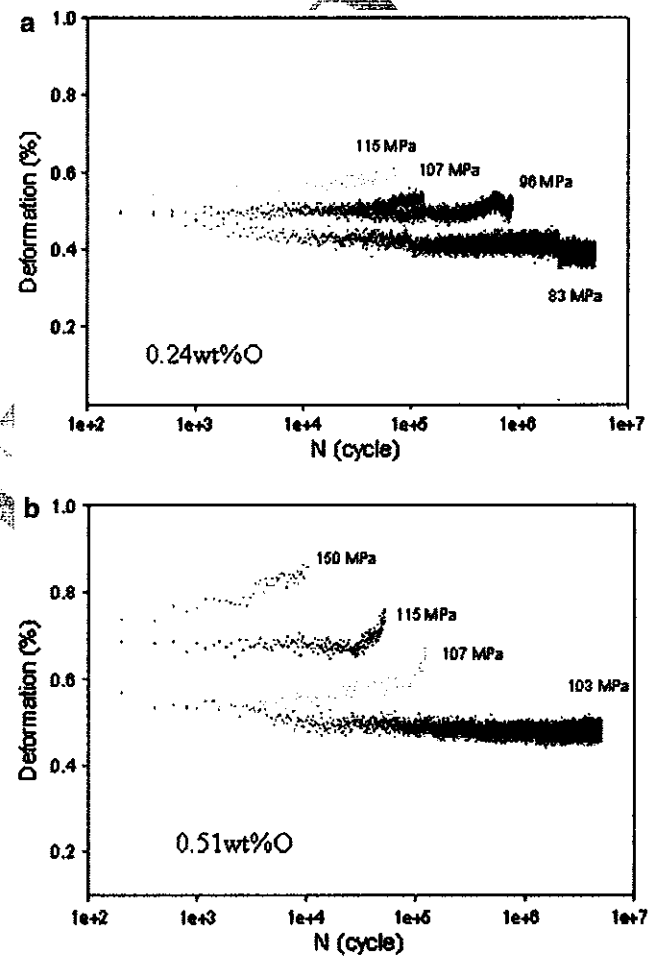

Fig. 9 Deformation amplitude versus cycle at different applied stresses for foams containing different amounts of oxygen in solution: **a** 0.24 and **b** 0.51 wt% O

10 Hz, $R = 0.1$) and tested at 107 MPa under static loading (creep) is presented in Fig. 12. The cyclic curve presents three stages (i.e. creep like, creep + initiation and propagation, crack coalescence). Beside, the static curve has only one and is linear. The slope of the static curve is similar to the slope of the initial portion of the cyclic curve.

The S–N curves for materials with three levels of oxygen in solution (0.24, 0.42 and 0.51 wt% O) is presented in Fig. 13. The number of cycles to failure criteria is defined as the intersection of the lines adjacent to the first and third stage of the cumulative deformation vs. cycle curves. No clear difference between the three series of

Journal : Large 10856 Dispatch : 10-6-2009 Pages : 11
Article No. : 3798 LE TYPESET

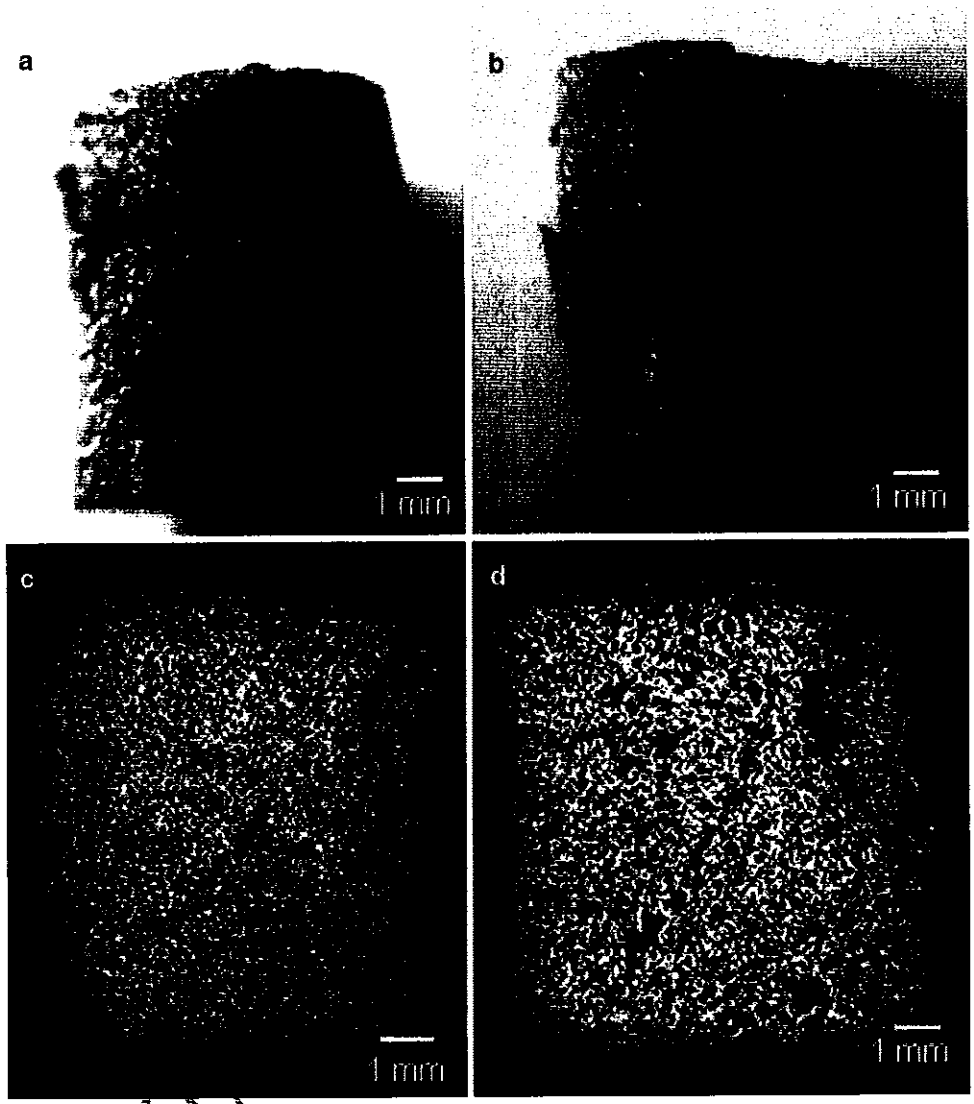

Fig. 10 Specimens at the end of the fatigue tests at 107 MPa (22.5% total deformation): **a** general view of the 0.24 wt% O specimen, **b** general view of the 0.51 wt% O specimen, **c** internal structure of a 0.24 wt% O specimen observed by microtomography, **d** internal structure of 0.51 wt% O specimen observed by microtomography

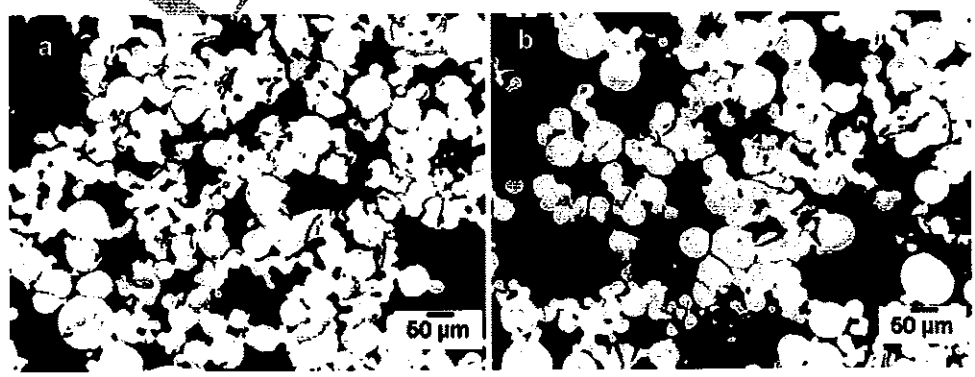

Fig. 11 Polished cross sections of the specimens at the end of the fatigue tests at 107 MPa (22.5% total deformation): **a** 0.24 wt% O specimen and **b** 0.51 wt% O specimen (arrows are pointing at microcracks)

specimens, containing 0.24, 0.42 and 0.51 wt% O, is observed in Fig. 12a. When all the specimens are considered, the fatigue limit all fitted in the 92 MPa ± 12 MPa range. The normalized S–N curves presented in Fig. 12b suggest a difference in fatigue behavior between the lowest and highest oxygen contents (0.24 vs. 0.51 wt% O). It should be noted that the specimens containing 0.42 and 0.51 wt% O did not show a different behavior in fatigue, probably as a result of their yield strengths that did not differ significantly (approximately 10%).

The fracture surface observed on specimens containing 0.24 and 0.51 wt% O (Fig. 14) shows that in both cases,

Journal : Large 10856 Dispatch : 10-6-2009 Pages : 11
Article No. : 3798 LE TYPESET
CP DISK

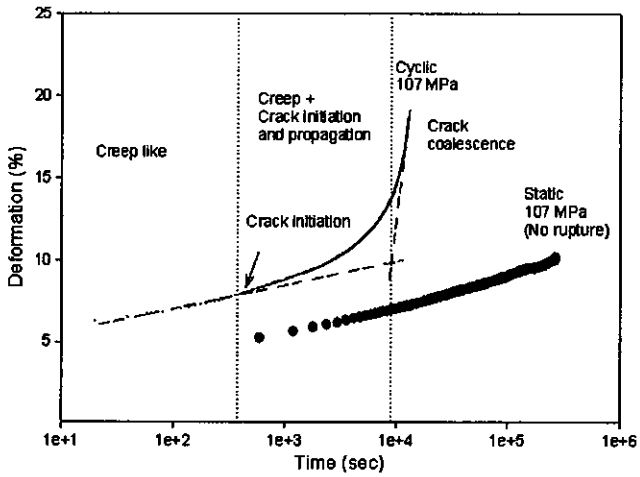

Fig. 12 Cumulative deformation versus time curves for specimens containing 0.24 wt% O in solution under two different charging modes: static (i.e. creep) and dynamic (10 Hz, $R = 0.1$)

quasi-cleavage is observed. However, ductile dimples were also observed on the fracture surface of the specimens with the lower oxygen content (i.e. 0.24 wt% O). This is consistent with observations done under monotonic compression testing [21].

4 Discussion

The amount of oxygen in solution has a clear effect on the compression behavior of the titanium foams under monotonic loading. While the smooth compression curves suggest that both materials are ductile, the specimens with smaller oxygen content (i.e. 0.24 wt% O) were significantly more ductile, which limited considerably the formation of cracks during monotonic deformation. The titanium foams containing larger amount of oxygen are more brittle, which leads to the formation of cracks that propagate during deformation. The formation of cracks and the damage of the specimens during monotonic compression postpone the densification stage and cause the slope of the densification stage to be smaller (Fig. 4). Indeed, the effective cross section of the specimen contributing to the densification at the end of the tests was smaller in the brittle specimens.

The increase of the yield strength with the oxygen content is consistent with observations done on dense titanium where the yield strength ($\sigma_{0.2}$) in tension typically increases from 170 to 480 MPa when the oxygen content increases from 0.18 to 0.4 wt%. Direct comparison cannot, however, be done since the deformation mechanisms of porous materials in compression are very different from those observed during the deformation of dense materials in tension.

The cumulative cyclic deformation curves are composed of three stages. The first stage corresponds to a linear regime, where the average deformation is increasing at a constant rate and the deformation amplitude is relatively constant (Figs. 8, 9). The deformation rate during this stage is similar to the one observed during the creep test (Fig. 12). This suggests that "creep like" deformation or ratcheting occurs during the initial portion of the compression–compression fatigue tests. This behavior has been reported for other types of metallic foams [22]. The second stage of the cyclic loading curve is observed when the cumulative deformation rate increases and the curve deviates from linearity. During this stage, cracks are initiated at different locations in the specimens but do not propagate rapidly as a result of the heterogeneous structure of the foams. In the present case, cracks in cell walls are stopped by pores or windows in the structure. The rupture of the cell walls forces the redistribution of the internal load, which leads to the formation of new cracks. Eventually, the increased concentration of microcracks leads to crack coalescence and the rapid collapse of the specimens.

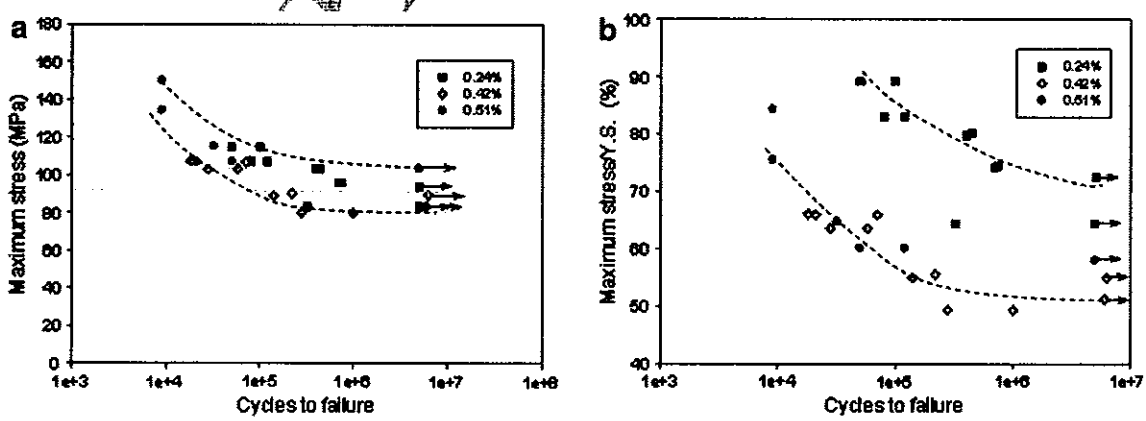

Fig. 13 Fatigue data for titanium foams with 0.24, 0.42 and 0.51 wt% oxygen in solution: **a** maximum stress and **b** maximum stress relative to the yield strength

Journal : Large 10856 Dispatch : 10-6-2009 Pages : 11
Article No. : 3798 LE TYPESET

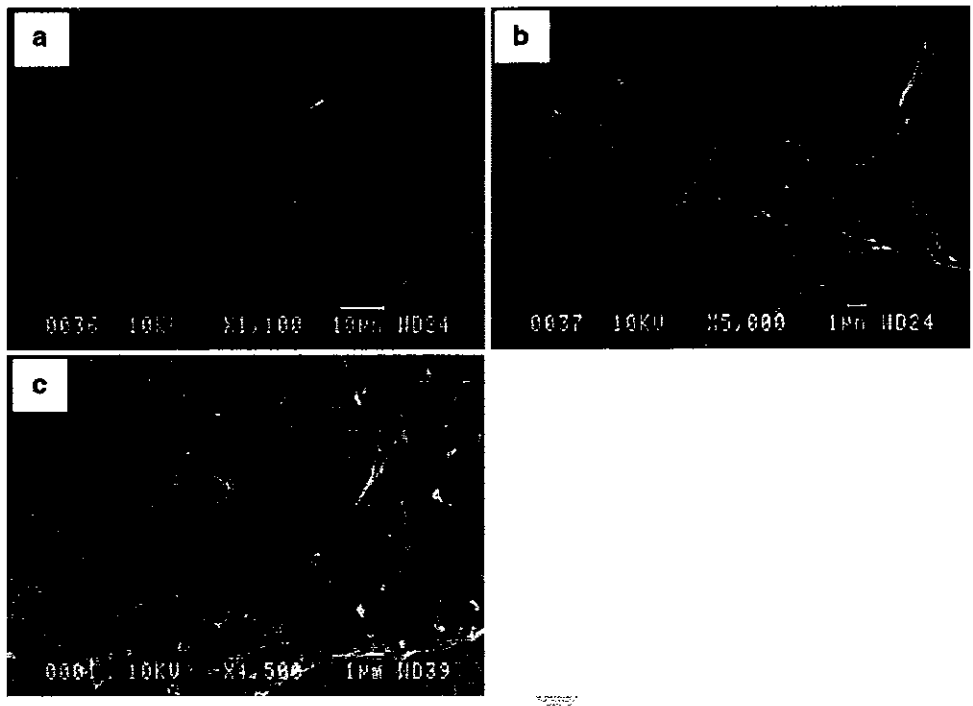

Fig. 14 Fracture surfaces after cycling **a** 0.24 wt% O in solution, **b** 0.24 wt% O in solution at higher magnification, **c** 0.51 wt% O in solution

This corresponds to the onset of the third stage observed in Fig. 8. While all specimens have cracks distributed in their structure after 22.5% of cyclic deformation, the presence of large cracks and the formation of debris during the tests were more important in the specimens containing higher oxygen content, due to their more brittle nature. Difference in ductility were in fact observed on the fracture surface of the specimens (Fig. 14). It was, however, difficult to extract much information from the fracture surfaces since the loading and deformation patterns in these porous materials are very complex and fracture surfaces are partially damaged during the tests.

The slope of the third stage is steeper in the foams with higher oxygen content, indicating a faster collapse in these specimens. While microcracks were observed in the specimens that failed during the cyclic tests at 107 MPa, microcracks were not observed in the specimens exposed to a 107 MPa static load for the same period of time. Accordingly, their formation is directly associated with the cyclic deformation mode observed during the fatigue tests.

It is recognized that porous metals and metallic foams behave differently than dense materials under static and cyclic loading. In foams, cyclic creep or ratcheting can be observed under non-zero mean stresses [22]. In compression-compression fatigue (load ratio >1), large cumulative plastic strains gradually develop and the material behaves in a quasi-ductile manner. The underlying mechanism is a combination of distributed cracking of the cell walls and edges and cyclic ratcheting under non-zero mean-stress leading to a progressive crushing of the cells [22].

The effect of the amount of oxygen in solution on the S–N curves (10 Hz, $R = 0.1$) is not important for the materials and oxygen range investigated in this study (i.e. 0.24–0.51 wt% O), despite the fact that the foams with higher content of oxygen are more brittle. However, when the maximum stress is divided by the yield strength of the foam, an effect of oxygen in solution can be observed. The relative fatigue limit of the 0.24 wt% O foams is approximately 70% of its yield strength while that of the 0.51 wt% O foam is approximately 52% of its yield strength. These observations suggest that the fatigue limit is not only affected by the yield strength but also by the ductility. This finding differs from observations reported in the literature on dense titanium in tension, where fatigue limit are generally 65-70% of the yield strength of the materials. For example, Lutjering and Williams [23] showed that the high cycle fatigue in tension ($R = -1$) at 10^7 cycles of grade 3 (0.35 wt% O) and grade 4 (0.4 wt% O) titanium increases with the oxygen content and that the fatigue strength is approximately 70% of the yield strength of the material. Wagner and Bigoney [24] observed that the high cycle fatigue resistance of titanium increases from 145 to 320 MPa when the oxygen content ranged from 0.13 to 0.46 wt%. Conrad [3] compiled the results from various investigators on the fatigue limit of dense titanium with oxygen content varying between 0.1 and 0.37 wt% O and showed that the fatigue limit is generally around 65% that of the yield strength.

This difference between the fatigue behavior in tension of dense titanium and that of titanium foams under

Journal : Large 10856 Dispatch : 10-6-2009 Pages : 11
Article No. : 3798 LE TYPESET

compression may be attributed to the different deformation modes observed. During cyclic loading of metallic foams under compression, the stresses are not uniformly distributed in the specimens and lead to simultaneous compression, tension and shear loading. Fatigue cracks are formed in various areas of the foam depending of the local load path. The failure of a cell wall forces the load path to be transferred to other portions of the specimen. Due to this mechanism, the specimen can support a significant number of cycles before failure occurs. However, when a sufficiently high density of microcracks is reached, crack coalescence is observed, which leads to the formation of larger cracks, generally at 45° with respect to the loading direction. Portions of the structure can then detach and be ejected, which leads to a reduction of the specimen cross section. This second failure mechanism could explain the influence of ductility on the fatigue behavior of titanium foam and, therefore, the effect of oxygen on the relative fatigue limit.

The fatigue limit at 5×10^6 cycles of the specimens characterized in this study fits in the 92 MPa $\pm$ 12 MPa range. These values are significantly larger than those observed with other metallic foams (Ta and Ni–Ti) intended for orthopedic applications [16–19]. This may be partially attributed to the higher relative density of the specimens characterized in this study. The values obtained are also significantly larger than the fatigue limit observed for dense cortical bone [25–27] and should be sufficient for the design of various structural and load bearing biomedical devices. Besides, the fatigue limit cannot be simply predicted from the yield strength of the material since the fatigue limit is not only linked to the yield strength of the material.

5 Conclusions

Titanium foams with different oxygen contents were characterized to evaluate the effect of oxygen on their compression behavior under static and cyclic loading. While the results obtained showed that oxygen in solution has a significant impact on the yield strength and the ductility of the foams, the effect of oxygen on the S–N curves (10 Hz, $R = 0.1$) is not important for the materials and oxygen range investigated in this study (i.e. 0.24–0.51 wt% O). This is attributed to the combined effect of the increased yield strength and the reduction of the ductility when the oxygen content increases. This finding differs from observations reported in the literature on dense titanium in tension, where fatigue limits are approximately 65–70% of the yield strength of the materials. During cyclic loading, the deformation of the foams is a combination of creep-like deformation and fatigue. During the initial stage of deformation, creep-like or ratcheting is the predominant deformation mechanism up to the appearance of microcracks distributed uniformly in the specimens. The coalescence of the cracks appears to be the governing mechanism for the final failure of the specimens. The fatigue limit at 5×10^6 cycles in the range 92 MPa $\pm$ 12 MPa were obtained for all specimens characterized in this study. This is significantly larger than the fatigue limit generally observed on other metallic foams intended for orthopedic applications as well as on dense cortical bone.

Acknowledgments The authors would like to acknowledge J.-P. Nadeau, S. Mercier, M. Plourde, D. Simard, F. Borgis and Dr. S. Lang for their contributions in the experimental work.

References

1. Cameron HU, Pilliar RM, McNab I. The effect of movement on the bonding of porous metal to bone. J Biomed Mater Res. 1973;7(4):301–11.
2. Bobyn JD, Pilliar RM, Cameron HU. The optimum pore size for the fixation of porous surfaced metal implants by the ingrowth of bone. Clin Orthop Relat Res. 1980;150:263–70.
3. Conrad H. Effect of interstitial solutes on the strength and ductility of titanium. Prog Mater Sci. 1981;26:123–403.
4. Murray JE, Wriedt HA. The O–Ti (oxygen–titanium) system. Bull Alloy Phase Diagrams. 1987;8:148–65.
5. Ottaviani G, Nava F, Quierolo G, Iannuzzi G, De Santi G, Tu KN. Low temperature oxygen dissolution in titanium. Thin Solid Films. 1987;146:201–7.
6. Wasz ML, Brotzen FR, McLellan RB, Griffin AJ Jr. Effect of oxygen and hydrogen on mechanical properties of commercially purity titanium. Int Mater Rev. 1996;41(1):1–12.
7. ASTM standard F 67-00, Standard Specification for Unalloyed Titanium, for Surgical Implant Applications (UNS R50250, UNS R50400, UNS R50550, UNS R50700).
8. ASTM standard F 1341-99, Standard Specification for Unalloyed Titanium Wire UNS R50250, UNS R50400, UNS R50550, UNS R50700).
9. ASTM standard F 1108-97a, Standard Specification for Titanium and Titanium-6 Aluminum-4 Vanadium Alloy Casting for Surgical Implants (UNS R56406).
10. ASTM standard F 136-98, Standard Specification for Wrought Titanium-6 Aluminum-4 Vanadium ELI (Extra Low Interstitial) Alloy (UNS R56401) for Surgical Implant Applications.
11. ASTM standard F 1472-02a, Standard Specification for Wrought Titanium-6 Aluminum-4 Vanadium Alloy for Surgical Implant Applications (UNS R56400).
12. ASTM standard F 1580-01, Standard Specification for Titanium and Titanium-6 Aluminum-4 Vanadium Alloy Powders for Coatings of Surgical Implants.
13. Yue S, Pilliar RM, Weatherly GC. The fatigue strength of porous-coated Ti-6Al-4V implant alloy. J Biomed Mater Res. 1984;18:1043–58.
14. Cook SD, Georgette FS, Skinner HB, Haddad RJ Jr. Fatigue properties of carbon- and porous-coated Ti–6Al–4V alloy. J Biomed Mater Res. 1984;18(5):497–512.
15. Fragomeni JM. J Adv Mater. 2001;33:3.
16. Arciniegas M, Aparicio C, Manero JM, Gil FJ. J Eur Ceram Soc. 2007;27.

Journal : Large 10856 Dispatch : 10-6-2009 Pages : 11
Article No. : 3798 LE TYPESET

17. Sevilla P, Aparicio C, Planell JA, Gil FJ. J Alloy Comp. 2007;439:67.
18. Barrabés M, Sevilla P, Planell JA, Gil FJ. Mater Sci Eng C. 2008;28:23.
19. Zardiackas LD, Parsell DE, Dillon LD, Mitchell DW, Nunnery LA. Structure, metallurgy, and mechanical properties of a porous tantalum foam. J Biomed Mater Res. 2001; 58(2):180–7.
20. Lefebvre LP, Thomas Y. Method of Making Open Cell Material, US patent 6,660,224 B2, Dec. 9, 2003.
21. Lefebvre LP, Baril E. Effect of oxygen concentration and distribution of the compression properties of titanium foams. Adv Eng Mat. 2008;10(9):868–76.
22. Ashby MF, Evans A, Fleck NA, Gibson LJ, Hutchinson JW, Wadley HNG. Metal Foams. A design Guide. Cambridge: Butterworth Heinemann; 2000.
23. Lütjering G, Williams JC. Titanium. 2nd ed. Springer: Pirna; 2007. p. 188.
24. Ashby MF, Evans A, Fleck NA, Gibson LJ, Hutchinson JW, Wadley HNG. Metal foams. A design guide. Cambridge: Butterworth Heinemann; 2000.
25. Zioupos P, Gresle M, Winwood K. Fatigue strength of human cortical bone: age, physical, and material heterogeneity effects. J Biomed Mat Res A. 2008;86A(3):627–36.
26. Choi K, Goldstein SA. A comparison of the fatigue behaviour of human trabecular and cortical bone tissue. J Biomech. 1992;25:1371–81.
27. Carter DR, Hayes WC. Compact bone fatigue damage. I. Residual strength and stiffness. J Biomech. 1977;10:325–37.

Journal : Large 10856 | Dispatch : 10-6-2009 | Pages : 11
Article No. : 3798 | LE | TYPESET